Kinesin-dependent movement on microtubules precedes actin-based motility of vaccinia virus

Jens Rietdorf*, Aspasia Ploubidou*, Inge Reckmann, Anna Holmström, Friedrich Frischknecht, Markus Zettl, Timo Zimmermann and Michael Way†#

European Molecular Biology Laboratory, Meyerhofstrasse 1, 69117 Heidelberg, Germany
**These authors contributed equally to this work*
†Present address: Imperial Cancer Research Fund, 44 Lincoln's Inn Fields, London WC2A 3PX, UK
#e-mail: m.way@ICRF.icnet.uk

Vaccinia virus, a close relative of the causative agent of smallpox, exploits actin polymerization to enhance its cell-to-cell spread. We show that actin-based motility of vaccinia is initiated only at the plasma membrane and remains associated with it. There must therefore be another form of cytoplasmic viral transport, from the cell centre, where the virus replicates, to the periphery. Video analysis reveals that GFP-labelled intracellular enveloped virus particles (IEVs) move from their perinuclear site of assembly to the plasma membrane on microtubules. We show that the viral membrane protein A36R, which is essential for actin-based motility of vaccinia, is also involved in microtubule-mediated movement of IEVs. We further show that conventional kinesin is recruited to IEVs via the light chain TPR repeats and is required for microtubule-based motility of the virus. Vaccinia thus sequentially exploits the microtubule and actin cytoskeletons to enhance its cell-to-cell spread.

The ability of viruses to reach their site of replication after entry into the cell is an essential aspect of the infection cycle. In the case of herpes simplex virus and adenovirus, dynein-driven microtubule-dependent movement of viral capsids towards the centre of the cell plays an important role during the initial stages of infection[1–3]. Microtubules and the dynein–dynactin complex are also needed to establish the site of vaccinia virus replication and assembly at the microtubule organizing centre[4]. An equally important transport problem during viral infection is the ability of newly assembled virus particles to leave infected cells. This problem is more acute for viruses such as herpes simplex that have to be transported long distances from the cell body along the axon to the epidermis during reactivation of latent infection[5–8]. The size of most virus particles is, however, such that their outward movement to the cell periphery is unlikely to occur by diffusion alone and will also require interactions with the host cytoskeleton[7,8]. Perhaps the best-characterized example of cytoskeleton-driven virus motility in recent years is the actin-based motility of vaccinia virus[9].

Vaccinia has a complex morphogenesis that occurs in cytoplasmic virus factories usually found in the perinuclear region of infected cells[10]. The intracellular mature virus (IMV) is the first form of the virus to assemble and consists of a protein core encapsulating the DNA genome, which has been wrapped by a membrane cisterna originating from the intermediate compartment[11]. A small proportion of IMVs undergo an additional wrapping with a membrane cisterna derived from the *trans*-Golgi network to form intracellular enveloped particles of vaccinia virus[12] (IEVs). IEVs are thought to be propelled through the cytoplasm of infected cells on the tips of actin tails by the polymerization of actin filaments, until they contact the plasma membrane[13]. Subsequent fusion of the IEV with the plasma membrane results in the formation of the cell-associated enveloped virus (CEV), which remains attached to the plasma membrane, and the extracellular enveloped virus (EEV), which is released from the cell[14,15]. CEVs attached to the outside of the cell continue to extend on cellular projections that are driven by actin polymerization on the inner surface of the plasma membrane until they fall off and become EEVs[16].

Vaccinia strains that cannot form actin tails have a small-plaque phenotype on confluent cell monolayers, suggesting that actin-based motility of the virus is required for efficient cell-to-cell spread[17–19]. Vaccinia actin-tail formation depends on Src-family kinases and tyrosine phosphorylation of the integral IEV membrane protein A36R (ref. 20). Tyrosine phosphorylation of A36R results in recruitment of the adapter molecule Nck, WASP-interacting protein (WIP) and N-WASP, the last of which activates the actin-nucleating activity of the Arp2/3 complex[20,21]. Thus, it appears that vaccinia virus has evolved a mechanism to mimic receptor tyrosine kinase signalling pathways that normally regulate actin polymerization at the plasma membrane to form long, virus-tipped projections that enhance cell-to-cell spread[9].

Results

Vaccinia actin tails form only at the plasma membrane. To obtain further insights into the actin-based motility of vaccinia virus, we performed video analysis on infected osteosarcoma cells stably expressing green fluorescent protein (GFP) fused to β-actin. The tips of vaccinia-induced actin tails move with a maximal average speed of 0.18±0.05 μm s^{-1} ($n = 25$) (Fig. 1a). During our study, we noticed that actin tails were predominantly localized at the cell periphery and formed very rapidly. Confocal analysis on fixed infected cells expressing GFP–β-actin revealed that vaccinia actin tails were never observed deep in the cytoplasm of the cell but were localized at the plasma membrane during all stages of infection (Fig. 1b). Confocal analysis of fixed samples, however, does not rule out the possibility that vaccinia tails are initiated deep in the cytoplasm and rapidly moved to the plasma membrane. We therefore analysed the formation of new actin tails in live cells using wide-field volume-imaging methods to determine where in the cell they form. A wide-field volume-imaging approach ensures that rapid actin tail formation events are not missed while performing *Z* sections through the cell, because aquisition of single sections is faster, as compared to

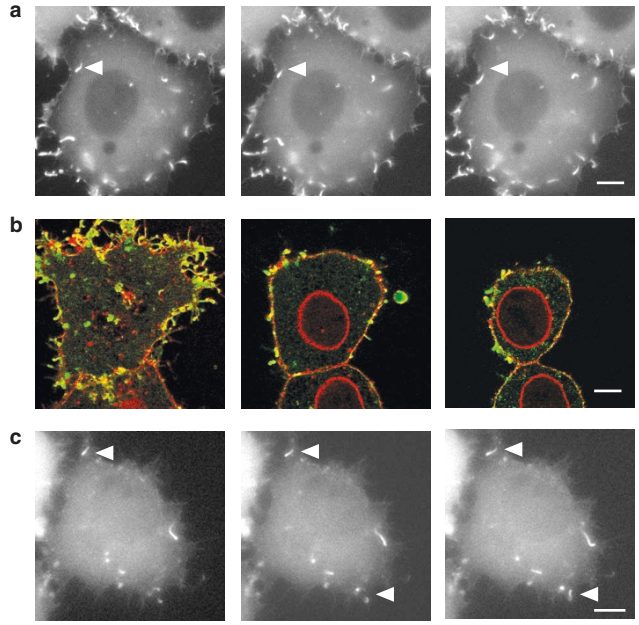

Figure 1 **Vaccinia actin tails are induced at and remain associated with the plasma membrane. a**, Movement of vaccinia-induced actin tails visualized with GFP–β-actin in an osteosarcoma cell 8 h after infection. The panels represent three images taken 10 s apart at a focal plane close to the cell substrate (see Movie 1). The white arrrowhead is in a fixed position. **b**, GFP–actin tails are located close to the plasma membrane. GFP–β-actin is green and the lectin stain of plasma and nuclear membranes is red. The left panel shows a confocal section near the cell substrate and the middle and right panels represent subsequent confocal sections with a depth of 0.8 μm spaced by 3.75 μm. **c**, Vaccinia actin tails form at the cell periphery. The panels represent three images taken 3 s apart of an osteosarcoma cell expressing GFP–β-actin 6 h after infection (see Movie 2). White arrowheads are in fixed positions, where the indicated actin tails initially form. Scale bars, 10 μm.

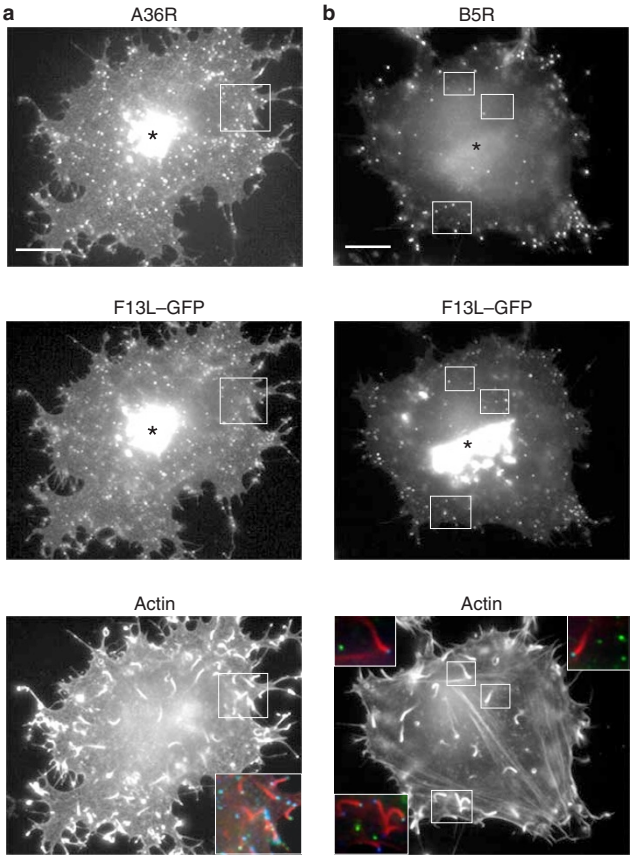

Figure 2 **Actin tails are formed beneath extracellular CEVs.** Immunofluorescence images of HeLa cells 8 h after infection. **a**, F13L–GFP (middle panel) is efficiently recruited to virus factories (indicated by the asterisks) and IEVs are labelled with anti-A36R antibody (left panel) and can be seen on the tips of actin tails, which are visualized with phalloidin (right panel). The insert shows an enlarged merged image of the area indicated by the box in the panels. In the merged image, A36R is in blue, F13L–GFP in green and actin filaments in red. **b**, Infected cells expressing F13L–GFP (middle panel) labelled with anti-B5R antibody before permeabilization (left panel) to distinguish between intra- and extracellular virus. B5R only labels extracellular CEVs, not virus factories or IEVs. By contrast, F13L–GFP is a marker for virus factories (indicated by the asterisks), intracellular IEVs and extracellular CEVs. The inserts show enlarged merged images of the areas indicated by the boxes in the panels. In the enlarged merged images, intracellular IEVs (green) are not associated with actin tails (red). By contrast, extracellular CEVs (cyan/white) are on the tips of actin tails (red). Scale bars, 10 μm.

confocal sectioning. Our analysis reveals that at least 83.4% ($n = 115$) of new events originate at the cell periphery or where the cell is in contact with the substrate, suggesting that actin tail formation occurs at or within 1.0 μm of the plasma membrane (Fig. 1c).

Vaccinia actin tails are nucleated by the extracellular CEVs. The observation that actin tails are associated only with the plasma membrane immediately raises the question of whether actin tails are induced by vaccinia before or after fusion of the IEV with the plasma membrane. We therefore examined whether actin tails were associated with IEVs in the cytoplasm and/or with the extracellular CEVs. CEVs are IEVs that have fused with the plasma membrane but remain attached to the outside of the cell[15].

Addressing this question requires the ability to distinguish between intracellular IEVs and extracellular CEVs during immunofluorescence analysis. We therefore took advantage of GFP to produce a tagged variant of the IEV-specific protein F13L (ref. 22). F13L–GFP was expressed during vaccinia infection to label IEVs without the need to permeabilize the cell during processing for immunofluorescence analysis. Western blot analysis of infected cells expressing F13L–GFP, with antibodies raised against amino (N) and carboxy (C)-terminal peptides of F13L, as well as anti-GFP antibody, reveals that the protein is the correct predicted size and is not degraded (data not shown). Immunofluorescence analysis of infected cells producing F13L–GFP reveals that the GFP-tagged protein is associated with virus factories and virus particles that are labelled with antibodies to the IEV-specific proteins A33R, A36R, B5R and F13L, as well as with virus particles inducing actin tails (Fig. 2a and data not shown). Our analysis indicates that F13L–GFP is a good marker for visualizing IEVs in live cells because it does not inhibit virus assembly or actin tail formation.

When infected cells are labelled with anti-B5R antibody without permeabilization, the extracellular CEVs are labelled but not the virus factories or IEVs, as would be observed using a standard permeabilization immunofluorescence protocol (Fig. 2b and data not shown). When infected cells producing F13L–GFP are labelled with anti-B5R antibody before permeabilization and afterwards stained with phalloidin to visualize actin, we observed that cytoplasmic IEVs, which are marked by F13L–GFP but lack B5R labelling, do not nucleate actin tails (Fig. 2b). In contrast, actin tails are observed in the cytoplasm immediately underneath the extracellular CEVs, which are labelled with both GFP and anti-B5R (Fig. 2b). Our data therefore indicate that actin tails form at the plasma membrane upon or after IEV fusion with the plasma membrane.

IEVs move to the cell periphery on microtubules. How do IEVs move from their perinuclear site of replication and assembly to the

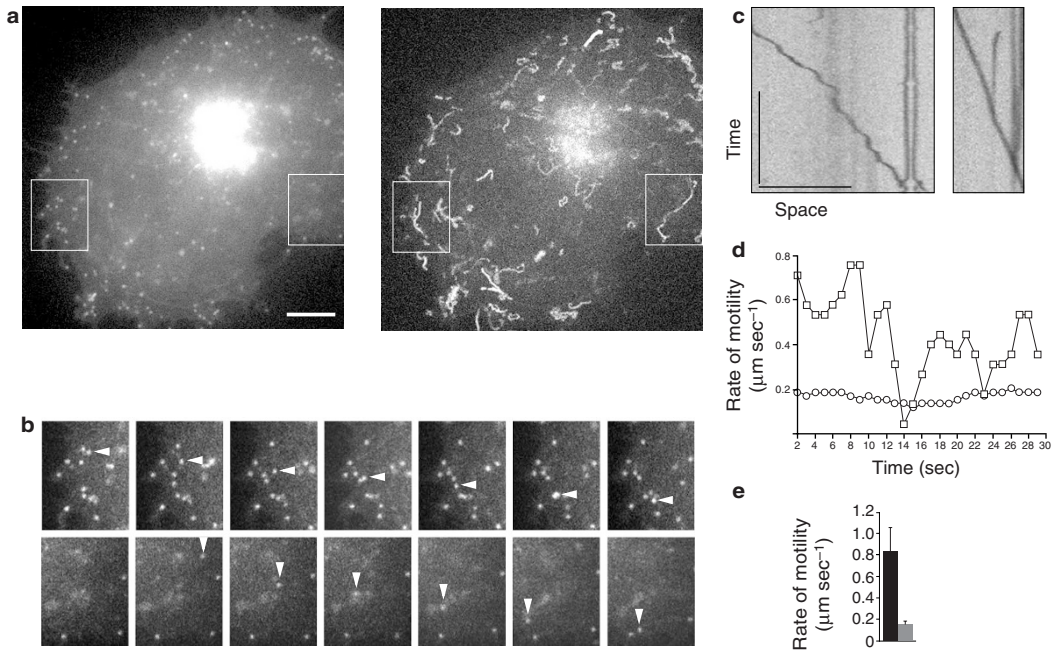

Figure 3 **Vaccinia virus exhibits both processive and saltatory movements.** Analysis of the movement of F13L–GFP-marked virus particles 8 h after infection. **a**, The left panel shows the first frame from the time lapse and the right panel shows the tracks taken by F13L–GFP-marked virus particles during 30 s (150 frames) of recording (see Movie 3). The boxes on the panels enclose the enlarged areas shown in **b**. Scale bar, 10 μm. **b**, Enlarged views showing that F13L–GFP-marked virus particles exhibit two distinct types of movement. In the upper row (left box in **a**), the particle indicated by the arrowhead represents a processively moving particle. In the lower row (right box in **a**), the vertical arrowhead indicates a virus particle moving in a non-processive or saltatory fashion. The panels represent still images taken from the video sequence at 1 s, 5 s, 10 s, 15 s, 20 s, 25 s and 30 s. **c–e**, Quantitative analysis of virus particle movements. **c**, Time–space plots representing changes of intensity along the tracks in **a** of the particles highlighted in **b**. The left panel represents saltatory particle movement and the right panel processive particle movement. Horizontal scale bar, 10 μm; vertical scale bar, 10 s. **d**, A graph of the instantaneous virus particle velocities extracted from **c**. **e**, Average maximal rates of movement for all virus particles analysed. The left column represents saltatory particle movement and the right column shows processive particle movement. Error bars represent standard deviation of the mean.

cell periphery in the absence of actin-based motility? To address this question we performed video analysis of infected cells expressing F13L–GFP as a reporter for IEVs. All F13L–GFP-labelled IEVs originated from the virus factories close to the nucleus. We found that there were two distinct types of IEV movement, processive and saltatory, in addition to the many non-motile particles (Fig. 3). The processive IEV movements are generally associated with the cell periphery as well as with virus-tipped projections. Analysis of their rate indicates that the processive IEVs have a maximal average speed of 0.15±0.03 μm s^{-1} ($n = 20$) (Fig. 3d,e). This is similar to the apparent rate observed for the tips of actin tails (0.18±0.05 μm s^{-1}), whose movement is also processive. Thus, the slower processive IEV movements are likely to represent the actin-based motility of virus particles.

The saltatory (in contrast to the processive) IEV movement occurs throughout the cell, often over long distances. Analysis of tracks reveals that saltatory IEV movements have a large range of instantaneous velocities (Fig. 3d). Therefore, to determine a meaningful rate for saltatory IEV movements that can be compared between different virus tracks and video sequences, we calculated the maximal velocity using the 25 frames surrounding the fastest instantaneous velocity value in the video sequences. The maximal average speed for saltatory IEV motion was 0.8 ± 0.2 μm s^{-1} ($n = 20$). The speed and behaviour of the faster IEV movements are reminiscent of microtubule-based motility of vesicles during membrane trafficking. Unfortunately, we could not perform drug inhibition studies to confirm that the faster movements are microtubule based because depolymerization of microtubules blocks IEV formation[4]. This is because microtubule depolymerization results in dispersion of the Golgi, which labels with IEV markers, throughout the cytoplasm[4,23]. We therefore performed real-time confocal video analysis on infected cells producing F13L–GFP and GFP–tubulin to visualize IEVs and microtubules directly (Fig. 4). Examination of the video sequences revealed that IEVs move on microtubules and even hop from microtubule to microtubule. In addition, we also performed image processing to separate moving IEVs from microtubules in order to facilitate visualization of their motion in static images (Fig. 4). Our data show that IEVs move along microtubules from a perinuclear region through the cytoplasm to the cell periphery, whereas actin tails move CEVs on the plasma membrane.

Vaccinia membrane protein A36R is required for IEV movement on microtubules. Previous studies have shown that the vaccinia integral membrane protein A36R is essential for actin-based motility but not for assembly of IEVs[18,19,24]. We therefore took advantage of the recombinant virus ΔA36R, which does not express the A36R protein, to study microtubule-based motility of IEVs in the absence of actin-based motility of CEVs. Unexpectedly, video analysis of cells infected with the ΔA36R virus strain expressing F13L–GFP revealed that IEVs remained in the perinuclear region and showed no sign of directed motility to the cell periphery (Fig. 5a). This observation suggests that A36R is required for both microtubule-mediated IEV movement and actin tail formation at the plasma membrane. In order to separate a role for A36R in microtubule-based motility from actin tail formation, we generated a recombinant virus A36R-YdF in which tyrosine residues 112 and 132 have been replaced by phenylalanine. We have previously shown that tyrosine phosphorylation of residues 112 and 132 of A36R are

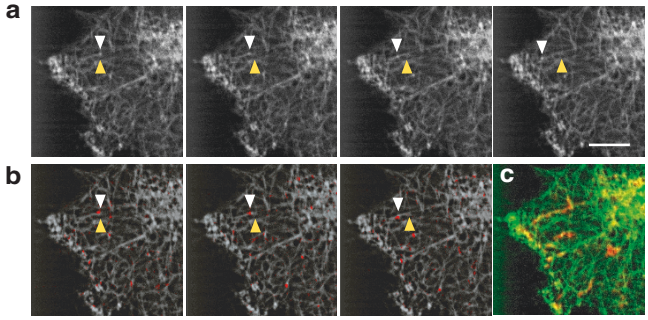

Figure 4 **IEVs move on microtubules.** Still images 5 s apart from confocal time-lapse recording of a HeLa cell expressing both tubulin–GFP and F13–GFP 8 h after infection. A single moving virus particle is indicated by the white arrowheads, with the original starting position indicated by the yellow arrowhead. **a**, GFP signals without separation of fast (virus) and slow (microtubule) movements (see Movie 4). **b**, The same images with separation to highlight the moving virus (red) on the more static microtubules (white). **c**, The tracks taken by the virus particle (red) extracted from 25 subsequent frames (20 s real time) superimposed on the underlying microtubules (green) (see Movie 5). Scale bar, 10 μm.

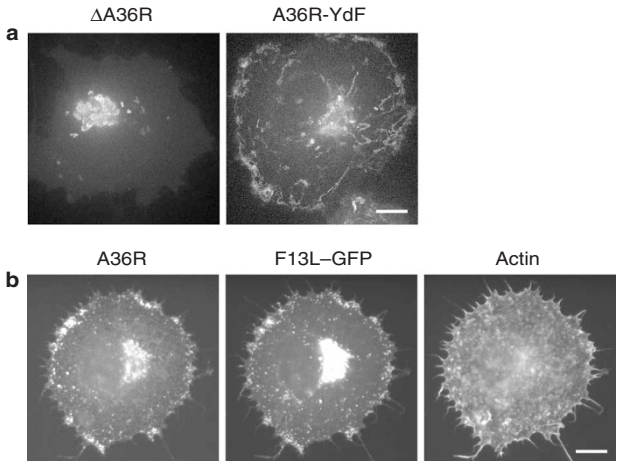

Figure 5 **A36R is required for microtubule-based motility of IEVs to the cell periphery. a**, Analysis of the movement of F13L–GFP-marked virus particles in ΔA36R and A36R-YdF infected HeLa cells 8 h after infection (see Movies 6 and 7). The tracks taken by F13L–GFP labelled virus are shown from 1 min (300 frames) of recording. IEVs lacking A36R (left) do not move to the cell periphery and remain at perinuclear virus factories. By contrast, A36R-YdF (right), which does not nucleate actin tails (**b**), can move to the cell periphery along microtubules. **b**, Immunofluorescence images of HeLa cells 8 h after infection reveal that recombinant A36R-YdF does not nucleate actin tails. A36R-YdF virus produces IEVs that are labelled with anti-A36R antibody (left) and recruit F13L–GFP (middle) but do not nucleate actin tails (right). Scale bars, 10 μm.

essential for actin tail formation but not for IEV assembly[20].

Immunofluorescence analysis of cells infected with vaccinia A36R-YdF with antibodies against the IEV-specific proteins A33R, A34R, A36R and F13L reveals that the virus makes IEVs that accumulate at the cell periphery but fail to make actin tails (Fig. 5b and data not shown). Furthermore, immunofluorescence analysis with anti-B5R antibody in the absence of cell permeabilization revealed that A36R-YdF can fuse with the plasma membrane to form CEVs even though no actin tails are observed (data not shown). Video analysis of cells infected with A36R-YdF and expressing F13L–GFP reveals that IEVs undergo long-range saltatory movements to the cell periphery but fail to exhibit any slow, processive, actin-driven movements (Fig. 5a and data not shown). An absence of slower, processive motility for A36R-YdF virus is consistent with its complete inability to form actin tails (Fig. 5b). The long-range saltatory movements have a similar maximal rate (0.8±0.2 μm s^{-1}, $n = 20$) as the parental Western Reserve (WR) strain (0.8±0.2 μm s^{-1}), indicating that they represent microtubule-based motility. Taken together, our data indicate that A36R is required for both microtubule- and actin-based motility.

Residues 71–100 of A36R are required for movement of IEVs to the cell periphery. To identify the region of A36R required for microtubule-based motility of IEV to the cell periphery, we initially produced a construct that expresses A36R tagged at its N or C terminus with GFP under the control of a synthetic early/late vaccinia promoter. We found that N-terminally tagged GFP–A36R was not functional and inhibited IEV formation (data not shown). By contrast, C-terminally tagged A36R–GFP, when expressed in cells infected with ΔA36R recombinant virus, was observed throughout the endoplasmic reticulum and was recruited to virus factories as well as to IEVs, which could move to the cell periphery to induce actin tails (Fig. 6 and data not shown). Thus, tagging A36R at its C terminus with GFP provides a good reporter because it does not inhibit IEV assembly, movement to the cell periphery or actin tail formation.

Previous studies have shown that residues 1–117 of A36R are sufficient for actin tail formation, albeit at reduced levels[20]. This region of A36R might therefore confer on IEVs the ability to move on microtubules, because it is reasonable to assume that this movement is a prerequisite for actin tail formation at the plasma membrane. We therefore examined the ability of a series of A36R C-terminal deletions (N100, N93, N81 and N72) tagged at their C terminus with GFP to rescue movement of the ΔA36R recombinant virus to the cell periphery, in order to determine which region of A36R is required for microtubule-based motility of IEVs (Fig. 6). Analysis of the C-terminal deletions reveals that residues 1–100 of A36R are sufficient to facilitate movement of IEVs to the cell periphery (Fig. 6). Although GFP-tagged A36R proteins smaller than residue 100 (for example, N93) could not rescue movement of the ΔA36R virus to the cell periphery, they were recruited to virus factories and IEVs (Fig. 6 and data not shown). The absence of IEV movement to the cell periphery in cells expressing smaller A36R constructs is not therefore a consequence of protein mistargeting. To delineate further the region responsible for mediating microtubule movements, we produced a series of internal deletions (TM53–100, TM63–100, TM71–100 and TM82–100) immediately after the transmembrane domain of A36R (residues 1–31) in the N100–GFP expression construct. We found that the internal deletion of residues 31–70 in N100–GFP did not inhibit the movement of IEV particles to the cell periphery. It was, however, noticeable that TM71–100 was not as efficient as N100 at mediating virus movement to the cell periphery (Fig. 6). Thus, residues 71–100 of A36R are minimally sufficient to facilitate outward movement of IEV particles to the cell periphery.

Conventional kinesin is required for microtubule-based motility of IEVs. Having determined that A36R is required for IEVs to move on microtubules *in vivo*, we sought to identify the microtubule motor responsible for this movement. Immunofluorescence analysis with the pan-kinesin HIPYR antibody failed to label IEVs (data not shown). By contrast, antibodies directed against the heavy and light chains of conventional kinesin readily labelled IEVs (Fig. 7a and data not shown). Conventional kinesin was, however, only observed on virus particles that had not nucleated actin tails (Fig. 7b). Furthermore, recruitment of conventional kinesin to IEVs was crucially dependent on A36R but independent of tyrosine phosphorylation on residues 112 and 132 (Fig. 7a).

To show that conventional kinesin is required for microtubule-based motility of IEVs, we examined the effect of overexpressing a GFP-tagged version of the TPR cargo-binding domain of kinesin light

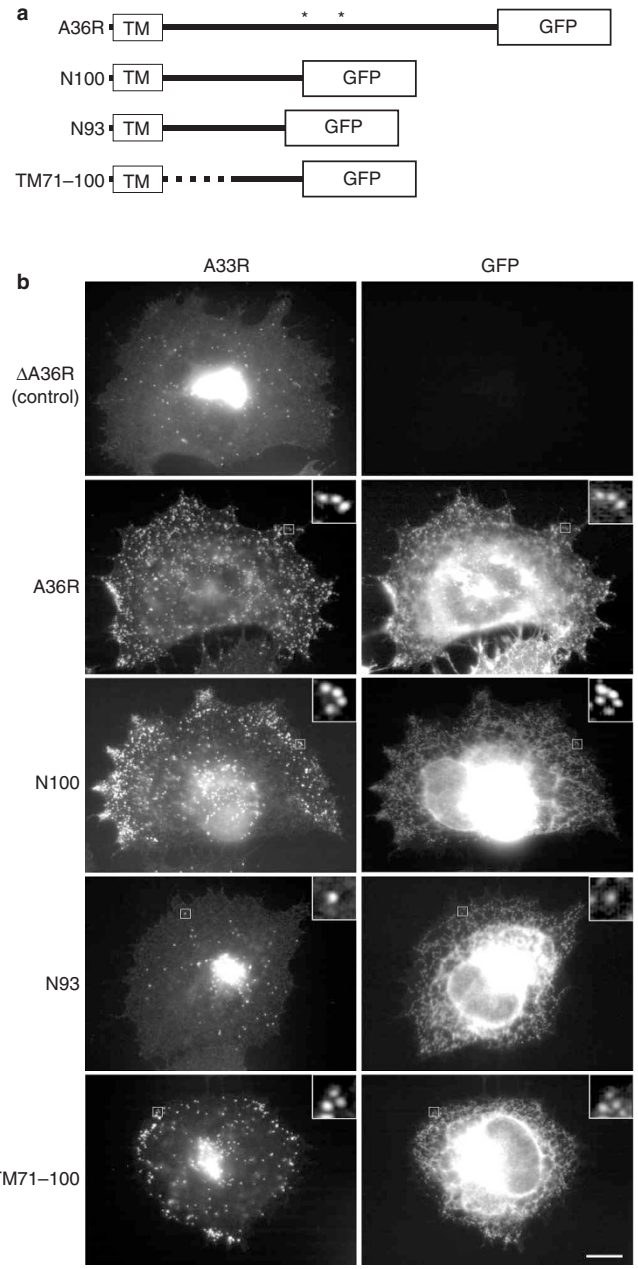

Figure 6 **Residues 71–100 of A36R are required for IEV dispersion to the cell periphery. a**, Schematic representation of the A36R expression constructs used (see Methods for nomenclature) to rescue dispersion of ΔA36R virus to the cell periphery. The box at the N terminus shows the predicted transmembrane domain (TM) and the C-terminal box indicates the GFP tag. The asterisks in the full-length protein indicate the positions of tyrosine 112 and 132, which are phosphorylated, and the dotted line in TM71–100 indicates the internal deletion in this construct. **b**, Immunofluorescence images of HeLa cells that have expressed the A36R–GFP-tagged constructs indicated on the left 8 h after infection with ΔA36R virus. The GFP (right) provides the marker for transfected cells and anti-A33R antibody (left) is used to visualize IEVs. Enlarged inserts show that the transfected constructs are incorporated into IEVs. Scale bar, 10 μm.

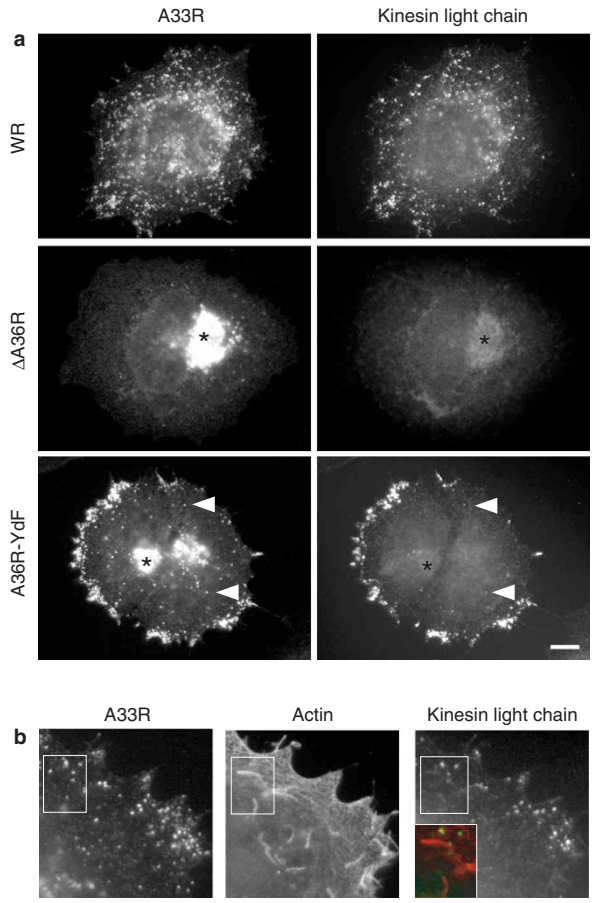

Figure 7 **Conventional kinesin is recruited to intracellular IEVs. a**, Immunofluorescence images of HeLa cells infected with WR, ΔA36R and A36R-YdF virus strains 8 h after infection labelled with anti-A33R antibody to visualize IEVs (left) and an antibody against conventional kinesin light chain (right). It is clear that only IEVs (arrowheads) and not perinuclear virus factories (indicated by the asterisks) recruit conventional kinesin. **b**, Immunofluorescence images of HeLa cells infected with WR and labelled with antibodies against A33R, actin and conventional kinesin light chain. The insert shows an enlarged merged image of actin in red and conventional kinesin light chain in green of the area indicated by the box in the panels. Scale bar, 10 μm.

chain 2 (KLC2)[25]. Western analysis of infected cells expressing GFP–KLC2–TPR with anti-GFP antibody reveals that the protein is the correct predicted size and is not degraded (data not shown). At low levels of expression, GFP–KLC2–TPR is recruited to IEVs (Fig. 8). Higher levels of GFP–KLC2–TPR expression resulted in 95.4 ± 0.1% inhibition of IEV accumulation in the cell periphery (Fig. 8), indicating that conventional kinesin is required for anterograde transport of IEVs.

Discussion

We have shown that actin tails are nucleated by the CEV at the plasma membrane and not by the IEV deep within the cytoplasm. Our previous electron microscopy study showed CEVs on the tips of actin projections but we assumed that these were formed by fusion of IEVs that had already nucleated actin tails in the cell cytoplasm[16]. Although we cannot rule out the possibility that actin tails do not form immediately before or during IEV fusion with the plasma membrane, we believe that they are most probably induced beneath extracellular CEVs, for the following reasons. First, we never observed by immunofluorescence cytoplasmic IEVs on actin tails, even though we would statistically have expected to have seen a few examples during our studies. Second, re-examination of unpublished electron micrographs from our earlier study failed to identify cytoplasmic IEVs on actin tails, although CEVs on the tips

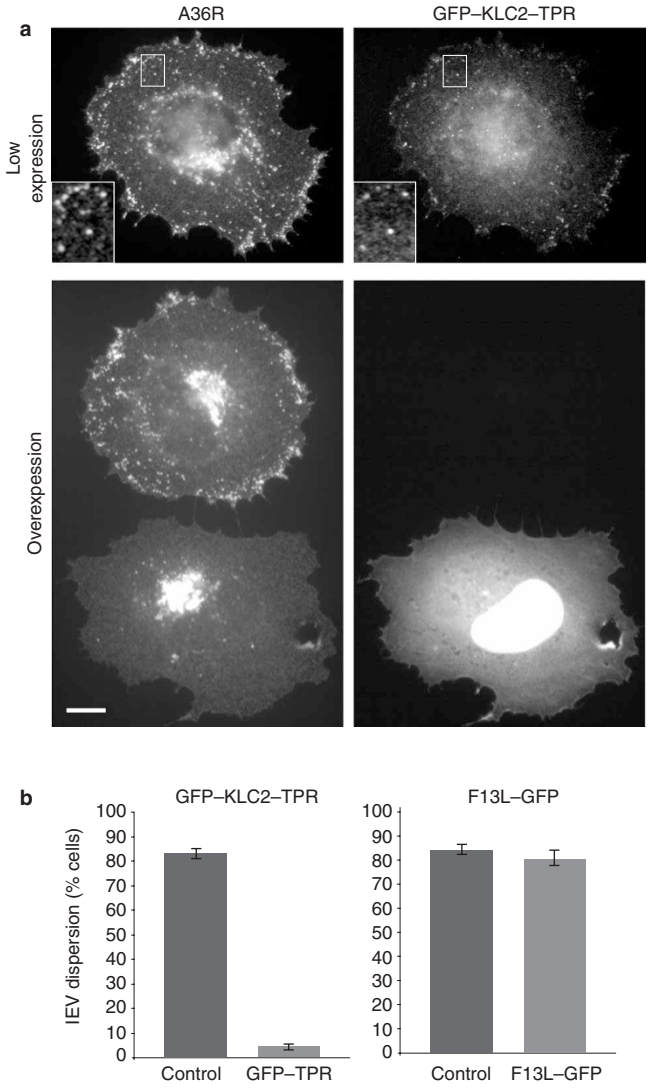

Figure 8 **Conventional kinesin is required for IEV motility to the cell periphery. a**, Immunofluorescence images) of HeLa cells infected with A36R-YdF expressing GFP–KLC2–TPR (right) 8 h after infection, also labelled with anti-A36R antibody to visualize IEVs (left). The enlarged inserts show that GFP–KLC2–TPR is recruited to IEVs at low levels of expression. At high GFP–KLC2–TPR expression levels (lower panels), IEVs do not move to the cell periphery. Scale bar, 10 μm. **b**, Quantification of IEV spread to the cell periphery in cells over expressing GFP–KLC2–TPR. The control represents untransfected but infected cells on the same coverslip as cells expressing GFP-tagged KLC2–TPR or F13L. Values represent the mean ± standard deviation from five independent experiments in which over 200 infected cells were examined for the accumulation of virus particles in the cell periphery in A36R-YdF infected cells.

of actin projections were readily observed[16]. Furthermore, CEVs are observed in cells infected with the recombinant vaccinia A36R-YdF, which does not induce actin polymerization, indicating that actin tail formation is not required for IEV fusion with the plasma membrane.

The fact that vaccinia only induces the formation of actin tails at the plasma membrane confirms previous suggestions[26–28]. It is also in agreement with the recent data from fixed preparations that actin tails are localized at the cell periphery, often with associated CEVs at their tips[23]. This study, although it is highly suggestive, does not formally rule out the possibility that vaccinia tails are initiated deep in the cytoplasm and rapidly end up at the plasma membrane. Our observations using wide-field volume-imaging methods on live cells, however, confirm that this is not the case and that actin tails only form close to the plasma membrane. This observation adds further support to the hypothesis that vaccinia actin tail formation mimics receptor tyrosine signalling cascades that lead to actin polymerization at the plasma membrane[20].

How does the CEV remain attached to the outside of the cell while, at the same time, A36R induces actin polymerization on the inner cytoplasmic surface of the plasma membrane? A36R is an integral membrane protein that has no lumenal tail and a cytoplasmic domain of ~190 amino acids on the outer surface of the IEV (refs 24,26,27). When the IEV fuses with the plasma membrane, the cytoplasmic domain of A36R remains exposed to the cytoplasm of the cell, where it can recruit the machinery required to nucleate an actin tail. A36R is, however, complexed to the integral IEV membrane proteins A33R and A34R, the latter of which is also associated with the IEV membrane protein B5R (refs 24,27). A33R, A34R and B5R, in contrast to A36R, have small cytoplasmic domains and large lumenal tails[24]. These lumenal tails become exposed on both the outer surface of the cell and the CEV when the IEV fuses with the plasma membrane. Interactions between these exposed lumenal tails in the plasma membrane and the CEV would allow virus particles to remain attached to the cell. Additional interactions between the C-type lectin domain in the lumenal tail of A34R exposed on the outer surface of the CEV with carbohydrates on the cell surface would also promote the retention of virus particles on the extracellular surface of the cell. Consistent with these suggestions, a naturally occurring point mutation in the carbohydrate-recognition domain of A34R (ref. 29), deletion of the A34R gene[30] and deletion of the complement consensus repeats in the lumenal tail of B5R (refs 31,32) all result in reduced retention of CEVs on the cell surface and increased virus release.

Although unexpected, vaccinia is not the first pathogen that has been found to induce actin polymerization on the inner surface of the plasma membrane while remaining on the outside of the cell. Enteropathogenic *Escherichia coli* (EPEC) and its close relative enterohaemorrhagic *E. coli* induce the formation of so-called actin pedestals[33,34]. EPEC pedestal formation depends on phosphorylation of tyrosine 474 of the bacterial protein Tir (translocated intimin receptor), which is inserted into the plasma membrane of the host cell by a type III secretion system[35,36]. Tyrosine phosphorylation of Tir results in recruitment of many cytoskeletal proteins, including Nck, N-WASP and the Arp2/3 complex, which are required for actin pedestal formation[9,37,38] [see Note added in proof]. The components recruited to EPEC pedestals and vaccinia actin tails are surprisingly similar, suggesting that both pathogens might induce actin assembly by a similar mechanism[9]. This is highly likely given that the sequence flanking Tyr112 of A36R, the phosphorylation of which is critical for vaccinia actin tail formation[20], is identical excluding a single residue to that around Tyr474 of Tir (ref. 9). Interestingly, vaccinia actin tails (virus particles) move at 0.15–0.18 μm s^{-1}, compared with 0.07 μm s^{-1} for EPEC (ref. 39). In this respect, the rate of actin-driven CEV movement is comparable to that of extracellular cationic beads (0.166±0.024 μm s^{-1}) on the surface of *Aplysia* bag cell growth cones, which are driven by so-called inductopodia that resemble actin tails[40].

In contrast to EPEC and polycationic beads, the question now remains as to why vaccinia actin tail formation only occurs at the plasma membrane and not on cytoplasmic IEVs, which have A36R on their surface. We know that vaccinia actin tail formation depends on Src-family kinases and that dominant negative c-Src is recruited to the site of actin tail formation[20]. Activated Src-family members that are associated with the plasma membrane are in the ideal position to phosphorylate A36R as the virus reaches the cell periphery and fuses with the plasma membrane but not before. However, we cannot exclude the possibility that activated Src at the plasma membrane might also locally phosphorylate and activate components that are found in the vaccinia actin tail cascade[9,20,21]. Tyrosine phosphorylation of N-WASP has yet to be described but

the related protein WASP can be tyrosine phosphorylated[41–43]. Although further work is required to understand why vaccinia actin tails only form at the plasma membrane, it is clear that microtubule-based movements provide the principal mechanism by which IEVs reach the cell periphery from their perinuclear site of replication and assembly[4]. If vaccinia was solely dependent on actin-driven movement in the cytoplasm, one would envisage that virus exit from the cell would be severely reduced because actin tails seem to lack directionality and would only occasionally take the virus to the plasma membrane. Using microtubules for long-range directed movement to the cell periphery and then using actin polymerization at the plasma membrane to provide the final push into neighbouring cells maximizes the use of the host cytoskeleton and provides an efficient, streamlined mechanism to ensure the continued spread of infection.

In contrast to actin-based motility, anterograde microtubule-based movement of IEVs is not processive and viral particles exhibit a range of motilities, often pausing. A similar observation of stop-and-start motility was recently reported for cytoplasmic IEV movements, although it was only suggested and not confirmed that this motility was microtubule based[28]. Similarly, it has been suggested that IEVs undergo stop–start microtubule-based motility, although the images presented in this study show processive movement (IEVs are equally spaced in time in Fig. 9)[23]. Microtubule-based motility in this study was inferred from microtobule depolymerization and from the co-localization of IEVs with microtubules in fixed preparations. We have, however, previously shown that depolymerization of microtubules with nocodazole inhibits IEV formation[4]. Furthermore, the presence of many virus particles and microtubules throughout the cell makes localization studies meaningless because particles will always appear to be close to microtubules given the inherent spatial resolution of the microscope. The definitive proof will only come from *in vitro* motility assays using pure components, although our observations of IEVs and microtubules simultaneously in live cells are highly suggestive.

IEV motility is very similar to that of membrane-bound vesicles, which display short-range or saltatory microtubule-based movement[44–46]. In addition, as with vesicular movements, the proportion of IEVs moving at any one time in an infected cell is small[44]. The average rate for saltatory IEV movements that we have measured at 0.8±0.2 $\mu m\ s^{-1}$ is within the range of values observed for the motility of motor-coated beads or from microtubule gliding assays using conventional kinesin from metazoans (0.5–1.0 $\mu m\ s^{-1}$)[47]. It is also in the range of the velocities for anterograde microtubule-based movement of herpes simplex virus[48].

Although we have learnt much over the past decade about conventional kinesin, we still know relatively little about the mechanism by which it is recruited to cargoes[44,49,50]. Our data clearly show that A36R is required for kinesin recruitment and is involved in microtubule-based motility of IEVs, in addition to its essential role in actin-based motility of IEVs (refs 18–20,24). This is in contrast to the conclusions of Hollinshead *et al.* (2001), who showed the presence of extracellular particles in ΔA36R-infected cells[23]. The reason for this difference requires further study but might be related to cell type and length of infection. Our studies with live cells were performed 6–8 h after infection on static cells, whereas the electron microscope studies of Holinshead *et al.* (2001) and Wolffe *et al.* (1998) were performed at 12 h and 24 h, respectively, by which time movement of the whole cell has occurred[51]. Furthermore, immuno-electron microscopy is required to determine the identity of these extracellular virus particles because IMVs can bud off under some situations[52].

Interestingly, our immunofluorescence data show that the A36R-dependent recruitment of conventional kinesin and actin tail formation are mutually exclusive, because we never see a virus particle associated with both kinesin and an actin tail. Therefore, A36R seems to provide a unique regulated link between the actin and microtubule cytoskeletons, although it shows no obvious sequence homology to any protein except for a small portion of Tir from EPEC. We have shown that residues 71–100 of A36R are sufficient to allow IEVs to reach the cell periphery. However, we have previously shown that residues 109–220 of A36R are sufficient to rescue actin tail formation by ΔA36R virus, albeit at only 21% of the level of full-length protein[20]. Assuming that diffusion plays little or no role, this suggests that a second region of A36R, in addition to the site we have mapped, can facilitate microtubule-based motility of IEVs. Residues 181–209 of A36R, which have limited sequence homology to residues 71–100, might be this second site. Further work is required to confirm whether this is indeed the case.

The fact that A36R-mediated recruitment of conventional kinesin, which is absolutely required for IEV movement to the cell periphery, occurs via the TPR repeats of the kinesin light chain (KLC) suggests that the molecular basis of recruitment resembles that mediated by amyloid precursor protein (APP) and Sunday Driver (SYD), both of which interact with the KLC (refs 53,54). This is in contrast to kinectin, which binds directly to the kinesin heavy chain[55]. APP and SYD have been shown to bind directly to the TPR repeats of the kinesin light chain[53,54] but residues 71–100 of A36R show no obvious sequence homology to APP or SYD, suggesting that A36R probably does not bind to a common sequence motif in the TPR repeats of KLC. Furthermore, we were unable to demonstrate a direct interaction between residues 71–100 of A36R and the TPR repeats of KLC using proteins produced in *E. coli* (M. Way, unpublished).

The most straightforward interpretation of these findings is that the interaction between A36R and the KLC TPR is not direct, and that additional components, either of host or viral origin, are required. A similar suggestion has recently been proposed for the recruitment of conventional kinesin by the JIP scaffolding protein complex to the Reelin receptor (ApoER2)[56]. An alternative explanation is that a post-translational modification of A36R, KLC or both proteins, which does not occur in *E. coli*, is required for a direct interaction to occur. Consistent with this notion, A36R has recently been shown to be heavily phosphorylated on serine, although the specific residues remain to be determined[27]. Furthermore, KLC has also been shown to be phosphorylated *in vivo*[57–60]. Although future studies will be directed at determining the molecular basis by which A36R recruits conventional kinesin, it is clear that motor recruitment is a tightly regulated process because virus factories, which contain exposed A36R, do not recruit conventional kinesin, even though IEVs do.

Our current understanding of the mechanism and regulation of the interaction of kinesin motors with their cargoes is limited[44,49,50]. Unravelling this complex problem is, however, essential if we are fully to understand the regulation of membrane trafficking. Vaccinia now provides not only a model system to dissect the mechanism of actin polymerization at the plasma membrane but also an amenable system to address microtubule-based motility and the regulation of motor function. Our data also raise the question of whether conventional kinesin-driven anterograde microtubule-dependent movements will emerge as a common mechanism used by viruses to leave the cell, just like dynein-based retrograde movements of viruses during the establishment of infection[7,8]. □

Note added in proof: Gruenheid *et al.* have recently shown that enteropathogenic *E. coli* Tir binds Nck to initiate actin pedestal formation in host cells (Gruenheid, S. *et al. Nature Cell Biol.* **3**, 856–859 (2001)).

Methods

Generation of stable GFP–β-actin cell lines.

The chicken β-actin gene was amplified by PCR using the primers 5′-CCCGCGGCCGCG-GAGGGATGGATGATGATAATGCTGCG-3′ (called Not-Act-For) and 5′-GGGGAATTCCTATTA-GAAGCATTTGCGGTGGAC-3′ (called Act-RI-Rev). The resulting PCR product was cloned into the *Not*I–*Eco*RI sites of the CMV transfection vector CB6N–GFP to generate CB6–GFP–β-actin, in which GFP is fused to the N terminus of actin by a short linker of glycine residues. CB6–GFP–β-actin was

transfected into NIH3T3 mouse fibroblasts and 143TK$^-$ human osteosarcoma cells using a standard calcium phosphate method and maintained in 0.5 μg active units of G418 (Geneticin) per ml or 0.3 μg active units of G418 per ml, respectively. In addition, 143TK$^-$ cells were maintained in 2.5% BM-Condimed H1 (Roche Diagnostics, Mannheim, Germany). Cells were sorted using fluorescence-activated cell sorting 12 days after G418 selection was applied and clonal cell lines were subsequently isolated by serial dilution.

pEL vector constructs.

The DNA corresponding to the F13L and A36R open reading frames was amplified from vaccinia genomic DNA by PCR using the primers 5′-GGGAAGCTTACCATGTGGCCATTTGCATCGGTAC-CTG-3′ (called F13L-H3-For), 5′-CCCCGCGGCCGCGCCGCCAATTTTTAACGATTTACTGTGGC-TAGA-3′ (called F13L-Not-Rev), 5′-GGGAGATCTACCATGATGCTGGTACCTCTTATC-3′ (called A36R-Bgl-For) and 5′-CCCCGCGGCCGCGCCGCCCACCAATGATACGACCGATGATTC-3′ (called A36R-Not-Rev). The resulting F13L PCR product was cloned into the *Hin*dIII–*Not*I sites of the vaccinia expression vector pEL (ref. 20), into which the gene for GFP had been inserted. The A36R PCR product was cloned into the *Bgl*II–*Not*I sites of the same vector. In the expression clones pEL–F13L–GFP and pEL–A36R–GFP, the C termini of F13L and A36R are linked to GFP by a short linker of glycine residues. C-terminal A36R deletion mutants fused to GFP were generated by introducing two glycine codons and a *Not*I site after the desired residue by PCR, and are named based on the remaining sequence, from the N terminus to their final C-terminal residue. To generate internal A36R deletions, we took advantage of a unique *Sna*B1 site that immediately follows the transmembrane domain of A36R (residues 1–32; TM). An in-frame *Sna*B1 site and two glycine codons were introduced by PCR immediately adjacent to the desired residue using A36R N100–GFP as a template. Internal deletion mutants are defined by the presence of TM followed by the residue positions in the cytoplasmic domain of A36R.

Residues 155–599 of the mouse KLC2, containing the TPR repeats[25], were amplified by PCR using the primers 5′-GGGGCGGCCGCGGCGGCAAGGGTGATGTCCCCAAAGACTCCCT-3′ (called KLC2-Not155-Fr) and 5′-CCCGAATTCAAAGTGCGGCTGTCAGAAAGACCCG-3′ (called KLC2-599 RI-Rv). The resulting PCR product was cloned into the *Not*I–*Eco*RI sites of pELGFP to generate N-terminally GFP-tagged KLC2–TPR. The fidelity of all expression clones used in this study was confirmed by sequencing.

Antibodies.

IEVs were labelled with antibodies against A33R, A34R and A36R (ref. 24), the rat monoclonal antibody 19C2 against B5R (refs 12, 61), or polyclonal antibodies raised against the F13L peptides CRL-VETLPENMDFRSDHL and CGFVSFNSIDKQLVSEAKK, corresponding to residues 14–30 and 339–356 of the protein. Both peptides were coupled, via the additional N-terminal cysteine introduced during synthesis, to Keyhole Limpet haemocyanin using the Imject activated immunogen conjugation kit (Pierce Chemical, Rockford, IL, USA). The conjugated peptides were separated from uncoupled peptide using a Presto desalting column (Pierce Chemical) and the pooled conjugates injected into rabbits. Anti-F13L antibodies were subsequently affinity purified on their respective peptides, which had been coupled via the N-terminal cysteine to SulfoLink columns (Pierce Chemical). The specificity of anti-F13L antibodies was confirmed by western and immunofluorescence analysis on HeLa cells infected with WR-strain virus expressing F13L–GFP.

Conventional kinesin was visualized with the monoclonal antibodies SUK4 (Covance, Richmond, CA, USA) or MAB1614 (H2) (Chemicon International, Temecula, CA, USA), directed against the heavy chain, or MAB1616 (L1) (Chemicon International), directed against the light chain. In addition, polyclonal sera against the kinesin light chain[25], a pan-KLC serum (35.1, Covance) and polyclonal sera against the heavy chain[53] were also used. The pan-kinesin heavy-chain polyclonal antibody HIPYER (ref. 62) was used to detect kinesin-family motors.

Actin was visualized with either the anti-β-actin antibody AC-74 (Sigma, Deisenhofen, Germany) or Alexa-488– or Texas-Red–phallicidin (Molecular Probes, Eugene, OR, USA). Microtubules were visualized by expressing mouse β-tubulin fused at its C terminus to EGFP using the expression vector pBactin-mb5tubulin-EGFP (A. Matus, unpublished).

Infection, pEL-driven expression and immunofluorescence on fixed preparations.

Cells were infected with WR and the recombinant vaccinia strain ΔA36R, which lacks the *A36R* gene[63]. Infected cells were fixed 6–8 h after infection and processed for immunofluorescence as described previously[21,24]. All pEL expression constructs were transfected 4–6 h after infection with WR, ΔA36R and A36R-YdF using lipofectin (Gibco–BRL) and processed for western blot or immunofluorescence analysis 2–4 h later. Alternatively, confocal sections of fixed, non-permeabilized infected cells expressing GFP–β-actin and labelled with wheat-germ agglutinin Alexa Fluor 594 (Molecular Probes) were taken on a Leica TCS SP2 confocal microscope using a 1.4 NA PlanApo objective lens, obtaining volume elements (voxels) measuring 66 × 66 × 200 nm ($x \times y \times z$).

Live cell imaging.

Cells were grown in glass-bottomed dishes (MatTek, Ashland, Maryland, USA) and maintained at 37 °C in CO_2-independent medium (MEM without phenol red but containing 30 mM Hepes (Gibco–BRL)) throughout the recording. Images were taken at 5 frames s^{-1} using an Olympus IX70 microscope with 1.2 NA UPlanApo PSF water immersion lens, a monochromator, a Piezzo stepper (Physik Instrumente, Waldbronn, Germany) and a camera controlled by TillVision software (Till Photonics, Martiensried, Germany). The pixel size was 111 nm^2. For volume imaging, stacks consisting of five planes spanning 10 μm above the coverglass were taken every second. For live cell confocal microscopy, images were taken from infected cells at 1.25 frames s^{-1} using an UltraView real-time confocal system (Perkin Elmer) using a Nikon 1.3 NA PlanFluar objective lens. The pixel size was 136 nm^2.

Image analysis.

For deconvolution and image reconstruction, image stacks were processed on a SGI Octane workstation running Huygens (Scientific Imaging, Leiden, The Netherlands) and Imaris (Bitplane, Zürich, Switzerland) software. Semi-automated particle tracking was performed using macros and routines for NIHimage (http://rsb.info.nih.gov/nih-image/) and Interactive Data Language (IDL, Research Systems, Boulder, Colorado, USA). The NIHimage macros used for this work can be downloaded from http://www.embl-heidelberg.de/~rietdorf/nihmacros.html. To calculate virus-particle velocities, subtraction images were automatically created for each time point of a time series by subtracting the preceding frame. Thus, particles changing their position between frames were highlighted while non-moving components of the image were suppressed. Virus particle trajectories were obtained by subsequent maximum intensity projection from the subtracted images. Along these trajectories, lines of grey value were read out for every image of a series and recombined into a new 'time–space plot'[64]. Velocities are read as changes in grey value over time from the time–space plots. Velocities were confirmed by manual tracking. A similar approach was used to image virus particles on microtubules more clearly. The highlighted moving particle images were overlaid on the original images in red to facilitate virus tracking on microtubules. To enhance the contrast of the microtubule signal (essentially static compared with the virus particles), a weighted walking average of three successive frames was used. This 'averaged' microtubule image was then recombined with the highlighted moving virus particles.

Construction of recombinant A36R-YdF vaccinia virus.

The pELA36R-YdF expression construct[20] was digested with *Kpn*1 and *Sca*I to release a fragment, corresponding to base pairs 14–438 of the *A36R* gene, which contains the tyrosine to phenylalanine mutations of residues 112 and 132. This fragment was cloned into the unique *Kpn*1 and *Sca*I sites of the plasmid pJEP2, which contains a 1584 bp fragment of vaccinia genomic DNA including the *A36R* gene[63]. The fidelity of the resulting construct (pJEP2-YdF) was confirmed by sequencing. pJEP2-YdF was transfected into HeLa cells 3 h after infection with ΔA36R (ref. 63), at a multiplicity of infection of 0.1 plaque-forming units. Two days later, cells were harvested and ruptured by freeze thawing. The cell lysate was then used to infect confluent BSC-1 cell monolayers, which were overlaid with 0.9% agarose 2 h after infection. Four days later, individual plaques were picked and the virus amplified by reinfecting HeLa cells for 48 h. The presence of *A36R* expression, which indicates the presence of a recombinant virus, in amplified samples was assessed by immunofluorescence analysis using antibodies against A36R (ref. 24). A36R-positive samples were subsequently plaque purified and amplified twice more until the recombinant virus (A36R-YdF) was clonal (i.e. all IEVs were A36R positive). To confirm the fidelity of the recombinant virus, DNA was prepared from infected cells and the complete region corresponding to the genomic region in pJEP2 was amplified by PCR using flanking primers. The resulting PCR product was cloned into pBluescript and the fidelity of the clone confirmed by sequencing.

RECEIVED 29 JUNE 2001; REVISED 25 JULY 2001; ACCEPTED 2 AUGUST 2001;
PUBLISHED 8 OCTOBER 2001.

1. Sodeik, B., Ebersold, M. W. & Helenius, A. Microtubule-mediated transport of incoming herpes simplex virus 1 capsids to the nucleus. *J. Cell Biol.* **136,** 1007–1021 (1997).
2. Suomalainen, M. *et al.* Microtubule-dependent plus- and minus end-directed motilities are competing processes for nuclear targeting of adenovirus. *J. Cell Biol.* **144,** 657–672 (1999).
3. Leopold, P. L. *et al.* Dynein- and microtubule-mediated translocation of adenovirus serotype 5 occurs after endosomal lysis. *Hum. Gene Ther.* **11,** 151–156 (2000).
4. Ploubidou, A. *et al.* Vaccinia virus infection disrupts microtubule organization and centrosome function. *EMBO J.* **19,** 3932–3944 (2000).
5. Holland, D. J., Miranda-Saksena, M., Boadle, R. A., Armati, P. & Cunningham, A. L. Anterograde transport of herpes simplex virus proteins in axons of peripheral human fetal neurons: an immunoelectron microscopy study. *J. Virol.* **73,** 8503–8511 (1999).
6. Miranda-Saksena, M., Armati, P., Boadle, R. A., Holland, D. J. & Cunningham, A. L. Anterograde transport of herpes simplex virus type 1 in cultured, dissociated human and rat dorsal root ganglion neurons. *J. Virol.* **74,** 1827–1839 (2000).
7. Sodeik, B. Mechanisms of viral transport in the cytoplasm. *Trends Microbiol.* **8,** 465–472 (2000).
8. Ploubidou, A. & Way, M. Viral transport and the cytoskeleton. *Curr. Opin. Cell Biol.* **13,** 97–105 (2001).
9. Frischknecht, F. & Way, M. Surfing pathogens and the lessons learned for actin polymerization. *Trends Cell Biol.* **11,** 30–38 (2001).
10. Tolonen, N., Doglio, L., Schleich, S. & Locker, J. K. Vaccinia virus DNA replication occurs in endoplasmic reticulum-enclosed cytoplasmic mini-nuclei. *Mol. Biol. Cell* **12,** 2031–2046 (2001).
11. Sodeik, B. *et al.* Assembly of vaccinia virus: role of the intermediate compartment between the endoplasmic reticulum and the Golgi stacks. *J. Cell Biol.* **121,** 521–541 (1993).
12. Schmelz, M. *et al.* Assembly of vaccinia virus: the second wrapping cisterna is derived from the *trans* Golgi network. *J. Virol.* **68,** 130–147 (1994).
13. Cudmore, S., Cossart, P., Griffiths, G. & Way, M. Actin-based motility of vaccinia virus. *Nature* **378,** 636–638 (1995).
14. Blasco, R. & Moss, B. Extracellular vaccinia virus formation and cell-to-cell virus transmission are prevented by deletion of the gene encoding the 37,000-Dalton outer envelope protein. *J. Virol.* **65,** 5910–5920 (1991).
15. Blasco, R. & Moss, B. Role of cell-associated enveloped vaccinia virus in cell-to-cell spread. *J. Virol.* **66,** 4170–4179 (1992).
16. Cudmore, S., Reckmann, I., Griffiths, G. & Way, M. Vaccinia virus: a model system for actin–membrane interactions. *J. Cell Sci.* **109,** 1739–1747 (1996).
17. Wolffe, E. J., Katz, E., Weisberg, A. & Moss, B. The *A34R* glycoprotein gene is required for induction of specialized actin-containing microvilli and efficient cell-to-cell transmission of vaccinia virus. *J. Virol.* **71,** 3904–3915 (1997).
18. Wolffe, E. J., Weisberg, A. S. & Moss, B. Role for the vaccinia virus A36R outer envelope protein in the formation of virus-tipped actin-containing microvilli and cell-to-cell virus spread. *Virology* **25,** 20–26 (1998).
19. Sanderson, C. M., Frischknecht, F., Way, M., Hollinshead, M. & Smith, G. L. Roles of vaccinia virus EEV-specific proteins in intracellular actin tail formation and low pH-induced cell–cell fusion. *J. Gen. Virol.* **79,** 1415–1425 (1998).
20. Frischknecht, F. *et al.* Actin-based motility of vaccinia virus mimics receptor tyrosine kinase signalling.

Nature **401,** 926–929 (1999).
21. Moreau, V. *et al.* A complex of N-WASP and WIP integrates signalling cascades that lead to actin polymerization. *Nature Cell Biol.* **2,** 441–448 (2000).
22. Hirt, P., Hiller, G. & Wittek, R. Localization and fine structure of a vaccinia virus gene encoding an envelope antigen. *J. Virol.* **58,** 757–764 (1986).
23. Hollinshead, M. *et al.* Vaccinia virus utilizes microtubules for movement to the cell surface. *J. Cell Biol.* **154,** 389–402 (2001).
24. Röttger, S., Frischknecht, F., Reckmann, I., Smith, G. L. & Way, M. Interactions between vaccinia virus IEV membrane proteins and their roles in IEV assembly and actin tail formation. *J. Virol.* **73,** 2863–2875 (1999).
25. Rahman, A., Friedman, D. S. & Goldstein, L. S. Two kinesin light chain genes in mice. Identification and characterization of the encoded proteins. *J. Biol. Chem.* **273,** 15395–15403 (1998).
26. van Eijl, H., Hollinshead, M. & Smith, G. L. The vaccinia virus A36R protein is a type Ib membrane protein present on intracellular but not extracellular enveloped virus particles. *Virology* **271,** 26–36 (2000).
27. Wolffe, E. J., Weisberg, A. S. & Moss, B. The vaccinia virus A33R protein provides a chaperone function for viral membrane localization and tyrosine phosphorylation of the A36R protein. *J. Virol.* **75,** 303–310 (2001).
28. Ward, B. M. & Moss, B. Visualization of intracellular movement of vaccinia virus virions containing a green fluorescent protein–B5R membrane protein chimera. *J. Virol.* **75,** 4802–4813 (2001).
29. Blasco, R., Sisler, J., R. & Moss, B. Dissociation of progeny vaccinia virus from the cell membrane is regulated by a viral envelope glycoprotein: effect of a point mutation in the lectin homology domain of the *A34R* gene. *J. Virol.* **67,** 3319–3325 (1993).
30. McIntosh, A. A. & Smith, G. L. Vaccinia virus glycoprotein A34R is required for infectivity of extracellular enveloped virus. *J. Virol.* **70,** 272–281 (1996).
31. Mathew, E., Sanderson, C. M., Hollinshead, M. & Smith, G. L. The extracellular domain of vaccinia virus protein B5R affects plaque phenotype, extracellular enveloped virus release, and intracellular actin tail formation. *J. Virol.* **72,** 2439–2438 (1998).
32. Herrera, E., del Mar Lorenzo, M., Blasco, R. & Isaacs, S. N. Functional analysis of vaccinia virus B5R protein: essential role in virus envelopment is independent of a large portion of the extracellular domain. *J. Virol.* **72,** 294–302 (1998).
33. Goosney, D. L., Gruenheid, S. & Finlay, B. B. Gut feelings: enteropathogenic *E. coli* (EPEC) interactions with the host. *Annu. Rev. Cell Dev. Biol.* **16,** 173–189 (2000).
34. Vallance, B. A. & Finlay, B. B. Exploitation of host cells by enteropathogenic *Escherichia coli. Proc. Natl. Acad. Sci. USA* **97,** 8799–8806 (2000).
35. Kenny, B. Phosphorylation of tyrosine 474 of the enteropathogenic *Escherichia coli* (EPEC) Tir receptor molecule is essential for actin nucleating activity and is preceded by additional host modifications. *Mol. Microbiol.* **31,** 1229–1241 (1999).
36. Frankel, G. *et al.* Intimin and the host cell—is it bound to end in Tir(s)? *Trends Microbiol.* **9,** 214–218 (2001).
37. Kalman, D. *et al.* Enteropathogenic *E. coli* acts through WASP and Arp2/3 complex to form actin pedestals. *Nature Cell Biol.* **1,** 389–391 (1999).
38. Goosney, D. L., DeVinney, R. & Finlay, B. B. Recruitment of cytoskeletal and signaling proteins to enteropathogenic and enterohemorrhagic *Escherichia coli* pedestals. *Infect. Immun.* **69,** 3315–3322 (2001).
39. Sanger, J. M., Chang, R., Ashton, F., Kaper, J. B. & Sanger, J. W. Novel form of actin-based motility transports bacteria on the surfaces of infected cells. *Cell Motil. Cytoskeleton* **34,** 279–287 (1996).
40. Forscher, P., Lin, C. H. & Thompson, C. Novel form of growth cone motility involving site-directed actin filament assembly. *Nature* **357,** 515–518 (1992).
41. Gross, B. S. *et al.* Regulation and function of WASp in platelets by the collagen receptor, glycoprotein VI. *Blood* **94,** 4166–4176. (1999).
42. Baba, Y. *et al.* Involvement of Wiskott–Aldrich syndrome protein in B-cell cytoplasmic tyrosine kinase pathway. *Blood* **93,** 2003–2012. (1999).
43. Guinamard, R., Aspenstrom, P., Fougereau, M., Chavrier, P. & Guillemot, J. C. Tyrosine phosphorylation of the Wiskott–Aldrich syndrome protein by Lyn and Btk is regulated by CDC42. *FEBS Lett.* **434,** 431–436 (1998).
44. Sheetz, M. P. Motor and cargo interactions. *Eur. J. Biochem.* **262,** 19–25 (1999).
45. Toomre, D., Keller, P., White, J., Olivo, J. C. & Simons, K. Dual-color visualization of trans-Golgi network to plasma membrane traffic along microtubules in living cells. *J. Cell Sci.* **112,** 21–33 (1999).
46. White, J. *et al.* Rab6 coordinates a novel Golgi to ER retrograde transport pathway in live cells. *J. Cell Biol.* **147,** 743–760. (1999).
47. Vale, R. D. *Kinesin, Conventional* (eds Kreis, T. & Vale, R.) 398–402 (Oxford University Press, 1999).
48. Penfold, M. E., Armati, P. & Cunningham, A. L. Axonal transport of herpes simplex virions to epidermal cells: evidence for a specialized mode of virus transport and assembly. *Proc. Natl. Acad. Sci. USA* **91,** 6529–6533 (1994).
49. Rogers, S. L. & Gelfand, V. I. Membrane trafficking, organelle transport, and the cytoskeleton. *Curr. Opin. Cell Biol.* **12,** 57–62 (2000).
50. Kamal, A. & Goldstein, L. S. Connecting vesicle transport to the cytoskeleton. *Curr. Opin. Cell Biol.* **12,** 503–508 (2000).
51. Sanderson, C. M., Way, M. & Smith, G. L. Virus-induced cell motility. *J. Virol.* **72,** 1235–1243 (1998).
52. Tsutsui, K. Release of vaccinia virus from FL cells infected with IHD-W strain. *J. Electron Microsc.* **32,** 125–140 (1983).
53. Kamal, A., Stokin, G. B., Yang, Z., Xia, C. H. & Goldstein, L. S. Axonal transport of amyloid precursor protein is mediated by direct binding to the kinesin light chain subunit of kinesin-I. *Neuron* **28,** 449–459 (2000).
54. Bowman, A. B. *et al.* Kinesin-dependent axonal transport is mediated by the sunday driver (SYD) protein. *Cell* **103,** 583–594 (2000).
55. Ong, L. L., Lim, A. P., Er, C. P., Kuznetsov, S. A. & Yu, H. Kinectin-kinesin binding domains and their effects on organelle motility. *J. Biol. Chem.* **275,** 32854–32860 (2000).
56. Verhey, K. J. *et al.* Cargo of kinesin identified as jip scaffolding proteins and associated signaling molecules. *J. Cell Biol.* **152,** 959–970 (2001).
57. Hollenbeck, P. J. Phosphorylation of neuronal kinesin heavy and light chains *in vivo. J. Neurochem.* **60,** 2265–2275 (1993).
58. Matthies, H. J., Miller, R. J. & Palfrey, H. C. Calmodulin binding to and cAMP-dependent phosphorylation of kinesin light chains modulate kinesin ATPase activity. *J. Biol. Chem.* **268,** 11176–11187 (1993).
59. Lee, K. D. & Hollenbeck, P. J. Phosphorylation of kinesin *in vivo* correlates with organelle association and neurite outgrowth. *J. Biol. Chem.* **270,** 5600–5605 (1995).
60. Lindesmith, L., McIlvain, J. M. Jr, Argon, Y. & Sheetz, M. P. Phosphotransferases associated with the regulation of kinesin motor activity. *J. Biol. Chem.* **272,** 22929–22933 (1997).
61. Hiller, G. & Weber, K. Golgi-derived membranes that contain an acylated viral polypeptide are used for vaccinia virus envelopment. *J. Virol.* **55,** 651–659 (1985).
62. Sawin, K. E., Mitchison, T. J. & Wordeman, L. G. Evidence for kinesin-related proteins in the mitotic apparatus using peptide antibodies. *J. Cell Sci.* **101,** 303–313 (1992).
63. Parkinson, J. E. & Smith, G. L. Vaccinia virus gene A36R encodes a *M,* 43–50 K protein on the surface of extracellular enveloped virus. *Virology* **204,** 376–390 (1994).
64. Siegert, F. & Weijer, C. J. Digital image processing of optical density wave propagation in *Dictyostelium discoideum* and analysis of the effects of caffeine and ammonia. *J. Cell Sci.* **93,** 325–335 (1989).

ACKNOWLEDGEMENTS
We thank L. Goldstein, G. B. Stokin and A. Kamal (UCSD, San Diego, USA) for antibodies against the heavy and light chains of conventional kinesin, as well as for the GST–KLC2 expression construct. We also thank A. Matus (Friedrich Miescher Institute, Basel, Switzerland) for providing his unpublished pBactin-mb5tubulin-EGFP expression vector and A. Desai (Max Planck Institute for Molecular Cell Biology and Genetics, Dresden, Germany) for the HIPYER antibody. We also thank I. Vernos, D. Brunner, F. Valderrama, E. Piddini and N. Scaplehorn for suggestions and comments concerning the manuscript. A. P. is supported by a European Commission Marie Curie Individual fellowship. A. H. is supported by Wenner-Gren Foundation (Sweden).
Correspondence and requests for materials should be addressed to M.W. Supplementary information is available on *Nature Cell Biology*'s website (http://cellbio.nature.com/).